

Made-to-measure galaxy models - II Elliptical and Lenticular Galaxies

R. J. Long^{1,2*} and Shude Mao^{1,2†}

¹*National Astronomical Observatories, Chinese Academy of Sciences, A20 Datun Rd, Chaoyang District, Beijing 100012, China*

²*Jodrell Bank Centre for Astrophysics, Alan Turing Building, The University of Manchester, Manchester M13 9PL, UK*

Accepted 2011 January 3. Received 2011 November 7; in original form 2011 August 8

ABSTRACT

We take a sample of 24 elliptical and lenticular galaxies previously analysed by the SAURON project using three-integral dynamical models created with Schwarzschild’s method, and re-analyse them using the made-to-measure (M2M) method of dynamical modelling. We obtain good agreement between the two methods in determining the dynamical mass-to-light (M/L) ratios for the galaxies with over 80% of ratios differing by $< 10\%$ and over 95% differing by $< 20\%$. We show that $(M/L)_{M2M} \approx (M/L)_{Sch}$. For the global velocity dispersion anisotropy parameter δ , we find similar values but with fewer of the made-to-measure models tangentially anisotropic by comparison with their SAURON Schwarzschild counterparts. Our investigation is the largest comparative application of the made-to-measure method to date.

Key words: galaxies: elliptical and lenticular – galaxies: kinematics and dynamics – galaxies: structure – methods: N-body simulations – methods: numerical

1 INTRODUCTION

Within the field of galactic and stellar dynamics, it has become common practice to model kinematic observations of a galaxy in order to interpret the observations and to understand better the underlying dynamical structures within the galaxy. Within this modelling arena, the method of Schwarzschild (1979) has been heavily developed and deployed with over 500 citations from other papers (for example, Rix et al. 1997, van den Bosch et al. 2008, Jalali & Tremaine 2011). By comparison, the made-to-measure method (M2M) formulated by Syer & Tremaine (1996) is less well-known but is no less capable, and has been the subject of growing interest recently (for example, Jourdeuil & Emsellem 2007, de Lorenzi et al. 2007, de Lorenzi et al. 2008, Dehnen 2009, Long & Mao 2010, Das et al. 2011). Both methods achieve their objectives by weighting a system of particles / orbits and superimposing them to reproduce the galactic observations. The key difference is that in Schwarzschild’s method a library of orbits is first created and then weighted, whereas in the M2M method the orbit weights are determined dynamically as the particles are being orbited. Other methods exist which, while not directly derived from Syer & Tremaine (1996), seek to tailor

the kinematics of a system of particles to match the kinematics of a galaxy, for example Rodionov et al. (2009).

In this paper we compare the made-to-measure method, as described by Long & Mao (2010), and Schwarzschild’s method. Cappellari et al. (2006) use Schwarzschild’s method to determine the mass-to-light ratios for a selection of galaxies observed with the SAURON¹ integral-field spectrograph. These same galaxies are re-analysed using the M2M method and the resulting ratios compared. The galaxies comprise a mixture of elliptical and lenticular galaxies covering both fast and slow rotators, and including both edge-on galaxies and galaxies inclined to the line of sight. As an extension to the mass-to-light exercise, we calculate the global anisotropy parameters as in Cappellari et al. (2007) and again compare the results. Earlier papers (for example, Das et al. 2011, or de Lorenzi et al. 2009) have used the M2M method effectively with individual galaxies. To our knowledge, this paper is the first to use the M2M method with a larger sample of galaxies and is the first to compare directly the results achieved with those from using Schwarzschild’s method.

In section 2 we describe the M2M method, and in section 3 its application to the SAURON galaxies. Sections 4 and 5 cover respectively the mass-to-light determinations and the global anisotropy parameters. We draw the activities to a conclusion in section 6. As might be expected, we

* E-mail: rjl2007@gmail.com

† E-mail: smao@nao.cas.cn

¹ Spectrographic Areal Unit for Research on Optical Nebulae

refer heavily to the published SAURON material for data values. We do not however cover in detail any theory from the SAURON material unless there is some specific point to be made in relation to the M2M method. Unless otherwise stated we adopt the same modelling assumptions as Cappellari et al. (2006).

2 THE M2M METHOD

2.1 Outline

In brief, the M2M method is concerned with modelling stellar systems and individual galaxies as a system of test particles orbiting in a gravitational potential. Weights are associated with the particles and are evolved over many orbital periods such that, by using these weights, observational measurements of a real galaxy are reproduced. We expect that the weights themselves will have converged individually to some constant value. It is natural to relate the particle weights to the luminosity of a galaxy and then to consider how the galaxy's surface brightness and luminosity weighted kinematics could be generated using the particle system.

In the next section, based on Long & Mao (2010), we set out the theory underlying the M2M method.

2.2 Theory

For a system of N particles, orbiting in a gravitational potential, with weights w_i , the key equation which leads to the weight evolution equation is

$$F(\mathbf{w}) = -\frac{1}{2}\chi^2 + \mu S + \frac{1}{\epsilon} \frac{dS}{dt} + \sum_i^Q C_i \quad (1)$$

where χ^2 , S and C_i are all functions of the particle weights $\mathbf{w} = (w_1, \dots, w_N)$; t is time; and μ and ϵ are positive parameters. The equations governing weight evolution over time come from maximising $F(\mathbf{w})$ with respect to the particle weights ($\partial F / \partial w_i = 0 \quad \forall i$) and rearranging terms to give equations of the form

$$\frac{d}{dt} w_i = -\epsilon w_i G(\mathbf{w}). \quad (2)$$

The overall rate of weight evolution is controlled by ϵ . The precise form of the function $G(\mathbf{w})$ depends on the constraints C_i and is illustrated later (equation 9). The process being applied to χ^2 is one of regularised, parameterised constrained extremisation.

The χ^2 term in F arises from assuming that the probability of the model reproducing a single observation can be represented by a Gaussian distribution and then constructing a log likelihood function covering all observations. For K multiple observables, we take χ^2 in the form

$$\chi^2 = \sum_k^K \lambda_k \chi_k^2 \quad (3)$$

where λ_k are small, positive parameters whose role is explained in section 3.7.

$$\chi_k^2 = \sum_j^{J_k} \Delta_{k,j}^2 \quad (4)$$

and

$$\Delta_{k,j} = \frac{y_{k,j}(\mathbf{w}) - Y_{k,j}}{\sigma_{k,j}} \quad (5)$$

where $Y_{k,j}$ is the measured value of observable k at position j with error $\sigma_{k,j}$, and $y_{k,j}(\mathbf{w})$ is the model equivalent of $Y_{k,j}$.

$$y_{k,j}(\mathbf{w}) = \sum_i^N w_i K_{k,j}(\mathbf{r}_i, \mathbf{v}_i) \delta(i \in k, j) \quad (6)$$

where $K_{k,j}(\mathbf{r}_i, \mathbf{v}_i)$ is the kernel for observable k evaluated at position j for a particle with position \mathbf{r}_i and velocity \mathbf{v}_i . $\delta(i \in k, j)$ is a selection function and signifies that only particles which contribute to observable k at position j should be included in the calculation of $y_{k,j}$. We have listed the kernels required for this paper in section 3.6.

The entropy function S in F is

$$S(\mathbf{w}) = - \sum_i^N w_i \ln\left(\frac{w_i}{m_i}\right) \quad (7)$$

where m_i is taken as the initial value of a particle weight (in practice, we take $m_i = 1/N$). S is used for regularisation / smoothing purposes with the amount of regularisation being controlled by the parameter μ . The derivative term dS/dt indicates that over time we require the particle weights, and thus S , to be constant. As demonstrated in Long & Mao (2010), the term behaves as the constraint $dS/dt = 0$.

The functions C_i in F are additional constraints to be included in the maximisation of F . In this paper, we use only one such constraint which is that we require the model luminosity to match the luminosity (L) of the galaxy being modelled, that is $\sum L w_i = L$, or more concisely $\sum w_i = 1$. We therefore take

$$C_1 = -\frac{\lambda_{\text{sum}}}{2} \left(\sum_i^N w_i - 1 \right)^2 \quad (8)$$

where λ_{sum} is a positive parameter.

Given the definitions of χ^2 , S and C_i and noting that for the purposes of this paper we do not use regularisation ($\mu = 0$), $G(\mathbf{w})$ from equation 2 can now be written

$$G(\mathbf{w}) = \sum_k^K \lambda_k \frac{K_{k,j}}{\sigma_{k,j}} \Delta_{k,j} + \lambda_{\text{sum}} \left(\sum_i^N w_i - 1 \right) \quad (9)$$

where $K_{k,j}(\mathbf{r}_i, \mathbf{v}_i)$ has been abbreviated to $K_{k,j}$ and we have assumed that, for all observables, 1 particle contributes only at 1 position j .

Finally, model observables (and thus particle weights) are subject to noise as the numbers of particles contributing to the observables vary. This noise is suppressed by replacing $\Delta_{k,j}$ in $G(\mathbf{w})$ by an exponentially smoothed version $\tilde{\Delta}_{k,j}$ given by

$$\frac{d}{dt} \tilde{\Delta}_{k,j} = \alpha (\Delta_{k,j} - \tilde{\Delta}_{k,j}) \quad (10)$$

where α is a small positive parameter. The smoothed $\Delta_{k,j}$ can be used to calculate a smoothed version $\tilde{y}_{k,j}$ of the model observable,

$$\tilde{y}_{k,j} = Y_{k,j} + \sigma_{k,j} \tilde{\Delta}_{k,j}. \quad (11)$$

3 SAURON M2M MODELS

3.1 Galaxies and observables

The galaxies which we model are as in Cappellari et al. (2006) but with NGC 221 omitted since it is not part of the SAURON data release. The galaxies are listed in Table 1 together with the properties which are relevant to M2M modelling. As indicated earlier, the galaxies comprise a mixture of elliptical and lenticular galaxies covering both fast and slow rotators, and including both edge-on galaxies and galaxies inclined to the line of sight. The galaxies also exhibit various core features, for example kinematically distinct cores or counter rotating cores (Emsellem et al. 2004).

The inclinations and distances (distance modulus) to the galaxies are as per Cappellari et al. (2006) Table 1. We have not attempted to use M2M modelling to determine the inclinations. Within a M2M model, we employ Cartesian axes such that the positive x-axis points towards the observer and the $y - z$ plane represents the galaxy's on sky projection. We align the galaxies' photometric major axes to the model y-axis utilising position angles taken from Cappellari et al. (2007).

We take kinematic data for the galaxies from the SAURON data release (Emsellem et al. 2004). The data available are the line-of-sight mean velocity, velocity dispersion and the h_3 and h_4 Gauss-Hermite coefficients, all taken from a truncated Gauss-Hermite expansion of the line-of-sight velocity distribution (van der Marel & Franx 1993),

$$\text{losvd}(v) = \frac{\exp(-v_{\text{norm}}^2/2)}{\sigma\sqrt{2\pi}} \left[1 + \sum_{n=3}^4 h_n H_n(v_{\text{norm}}) \right] \quad (12)$$

where H_n is the Hermite polynomial of degree n and the normalised velocity v_{norm} is defined as

$$v_{\text{norm}} = \frac{v - \bar{v}}{\sigma} \quad (13)$$

where \bar{v} and σ are the line-of-sight mean velocity and velocity dispersion respectively.

The h_5 and h_6 Gauss-Hermite coefficients used in Cappellari et al. (2006) are not available in the data release. We assume therefore that $h_5 = h_6 = 0$ with a measurement error of ± 0.3 (M. Cappellari private communication). We do not model a galaxy's mean line-of-sight velocity and velocity dispersion directly but instead model $h_1 = h_2 = 0$ as in Rix et al. (1997). Following Magorrian & Binney (1994), we calculate the measurement errors Δh_1 and Δh_2 as

$$\Delta h_1 = -\frac{\Delta v}{\sqrt{2}\sigma} \quad (14)$$

and

$$\Delta h_2 = \frac{\Delta\sigma}{2\sigma} (\sqrt{12}h_4 - \sqrt{2}), \quad (15)$$

where Δv and $\Delta\sigma$ respectively are the measurement errors in the mean line-of-sight velocity v and velocity dispersion σ . If we require the model mean line-of-sight velocity v_m or the model line-of-sight velocity dispersion σ_m , we calculate them as

$$v_m = v - \sqrt{2}\sigma h_{1,m} \quad (16)$$

and

$$\sigma_m = \sigma + \frac{2\sigma h_{2,m}}{\sqrt{12}h_{4,m} - \sqrt{2}}, \quad (17)$$

where the $h_{i,m}$ are the exponentially smoothed model h_i values. de Lorenzi et al. (2009) use a similar approach in their M2M models of NGC 3379. It is possible to calculate v_m , σ_m and the Gauss-Hermite coefficients by fitting Gauss-Hermite series directly to the end of modelling run particle data, provided sufficient particles are available to populate the velocity histograms necessary to the fitting process. The approach above, using smoothed model values, avoids the need to run the M2M models with large numbers of particles.

We put the SAURON kinematic data through a cleaning process (section 3.3) before subtracting the systemic galactic velocity from the mean line-of-sight velocity, symmetrizing the data and converting it to units appropriate to our M2M modelling (distances in effective radii, time in 10^7 years). We take the systemic velocities from Emsellem et al. (2004) and assume they are subject to a measurement error of 10%. The usual error propagation rules are applied.

The observables in our M2M models are thus

- (i) surface brightness,
- (ii) Gauss-Hermite coefficients h_1 to h_6 .

Values for the kinematic observables are as described above, and surface brightness is calculated from the multi-Gaussian expansions of the galaxy's surface brightness (see section 3.4). For modelling purposes, we assume a 10% relative error in surface brightness values. Unless explicitly stated, luminosity density is not used in our M2M models to constrain the luminous matter distribution (see section 3.9).

Similarly to Cappellari et al. (2006), we perturb the line-of-sight particle coordinates by a 'point spread function' before binning any model data to create the model observables. We use the seeing values from Emsellem et al. (2004) Table 3 and implement the function as a circular Gaussian distribution.

3.2 Voronoi Tessellation

To achieve a pre-determined signal to noise, the SAURON observations were adaptively binned and processed, as described in Cappellari & Copin (2003) and Emsellem et al. (2004), resulting in a centroidal Voronoi tessellation. The kinematic data in the SAURON data release are presented in the context of that tessellation. The M2M models use the same Voronoi tessellation for determining model kinematic observables. The Voronoi cells are the bins used for accumulating particle kinematic data as part of the construction of the model observables.

Within our M2M implementation, the Voronoi bins are represented by a 2D 'tree' with a surrounding convex hull. Particles are binned by first determining whether they are inside the convex hull and, if they are, performing a 'nearest neighbour search' of the 2D tree to identify the bin required. The areas of the bins (needed for model observable calculations - see section 3.6) are calculated using a Monte Carlo approach. As an example, Figure 1 shows the positions of the Voronoi centroids (the data measurement points) for NGC 3156 together with their convex hull. The SAURON data release contains no information on the extent of the outermost

Table 1. Galaxy sample and measured parameters

Galaxy	Type	Fast rotator	Distance Mpc	R_e arcsec	σ_e km s ⁻¹	i deg	PA deg	Seeing arcsec	V_{sys} km s ⁻¹	$(M/L)_{\text{Schw}}$ I-band	$(M/L)_{\text{M2M}}$ I-band
(1)	(2)	(3)	(4)	(5)	(6)	(7)	(8)	(9)	(10)	(11)	(12)
NGC 524	S0 ⁺ (s)	yes	23.34	51	235	19	48.4	1.4	2353	4.99	6.39
NGC 821	E6?	yes	23.44	39	189	90	32.2	1.7	1722	3.08	3.37
NGC 2974	E4	yes	20.89	24	233	57	43.5	1.4	1886	4.52	4.60
NGC 3156	S0 :	yes	21.78	25	65	67	49.4	1.6	1541	1.58	1.46
NGC 3377	E5 – 6	yes	10.91	38	138	90	41.3	2.1	690	2.22	2.22
NGC 3379	E1	yes	10.28	42	201	90	67.9	1.8	916	3.36	3.67
NGC 3414	S0pec	no	24.55	33	205	90	179.9	1.4	1472	4.26	4.56
NGC 3608	E2	no	22.28	41	178	90	79.3	1.5	1228	3.71	3.73
NGC 4150	S0 ⁰ (r)?	yes	13.37	15	77	52	147.0	2.1	219	1.30	1.26
NGC 4278	E1 – 2	yes	15.63	32	231	45	16.7	1.9	631	5.24	5.61
NGC 4374	E1	no	17.87	71	278	90	128.2	2.2	1023	4.36	4.65
NGC 4458	E0 – 1	no	16.75	27	85	90	4.5	1.6	683	2.28	2.32
NGC 4459	S0 ⁺ (r)	yes	15.70	38	168	47	102.7	1.5	1200	2.51	2.76
NGC 4473	E5	yes	15.28	27	192	73	93.7	1.9	2249	2.91	3.12
NGC 4486	E0 – 1 ⁺ pec	no	15.63	105	298	90	158.2	1.0	1274	6.10	7.05
NGC 4526	SAB0 ⁰ (s)	yes	16.44	40	222	79	112.8	2.8	626	3.35	3.26
NGC 4550	SB0 ⁰ : sp	yes	15.42	14	110	84	178.3	2.1	413	2.62	2.78
NGC 4552	E0 – 1	no	14.93	32	252	90	125.3	1.9	351	4.74	5.01
NGC 4621	E5	yes	17.78	46	211	90	163.3	1.6	456	3.03	3.07
NGC 4660	E	yes	12.47	11	185	70	96.8	1.6	1089	3.63	3.85
NGC 5813	E1 – 2	no	31.33	52	230	90	134.5	1.7	1947	4.81	4.69
NGC 5845	E :	yes	25.24	4.6	239	90	143.2	1.5	1474	3.72	4.34
NGC 5846	E0 – 1	no	24.21	81	238	90	75.2	1.4	1710	5.30	5.38
NGC 7457	S0 ⁻ (rs)?	yes	12.88	65	78	64	125.5	1.3	845	1.78	1.52

Column (1): NGC number. Column (2): Hubble type from Emsellem et al. (2004). Column (3): Fast/slow rotator from Cappellari et al. (2006). Column (4): Distance calculated from distance modulus in Cappellari et al. (2006). Column (5): Effective (half-light) radius from Cappellari et al. (2006). Column (6): Velocity dispersion within effective radius from Cappellari et al. (2006). Column (7): Inclination from Cappellari et al. (2006). Column (8): Position angle from Cappellari et al. (2007). Column (9): Seeing from Emsellem et al. (2004). Column (10): Systemic velocity from Emsellem et al. (2004). Column (11): Schwarzschild mass-to-light ratio from Cappellari et al. (2006). Column (12): M2M mass-to-light ratio - section 4.

Voronoi bins, and, as a consequence, the model observable calculations for such bins are biased inwards. This is not considered a significant issue as the number of such bins is small.

Voronoi bins are not used with surface brightness. Instead we employ a 16×16 polar grid with radial divisions pseudo-logarithmic as described Long & Mao (2010).

To give an indication of the number of observations being modelled, of the 24 galaxies, NGC 5845 has the least number of Voronoi bins with 164 and NGC 4486 the greatest with 2112 bins. The total number of observations is therefore 1240 for NGC 5845 and 12,928 for NGC 4486.

3.3 Data cleaning

We have subjected the SAURON data release to a number of checks to eliminate suspect kinematic data

- (i) ‘nan’ (not a number) value check
- (ii) zero value check, for example error fields should not be zero
- (iii) positive value check, for example error fields should not be negative
- (iv) small value check ($< 10^{-5}$)
- (v) record sequence check - a record is flagged if a data

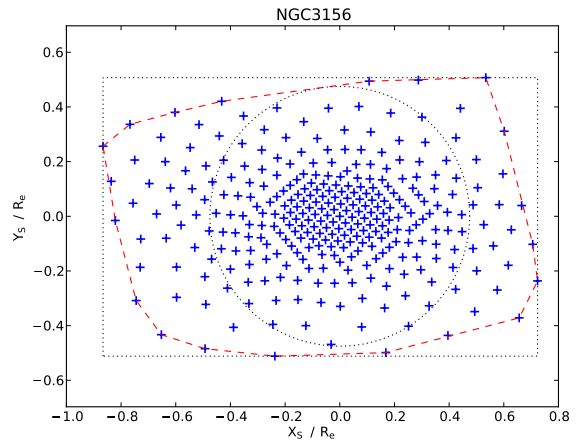


Figure 1. Measurement points (X_S, Y_S) are in blue and the convex hull is indicated by the red dashed lines. The bounding rectangle is used in calculating the bin areas. The circle has the maximum possible radius for a circle to lie within the convex hull, and is used for performance reasons as part of the algorithm to determine whether or not a particle is inside the hull or not. Distances are in units of effective radii R_e for the galaxy.

field in one record has the same value as in the previous record

Note that not all checks are applied to all data fields.

In total, 13 galaxies were found to have suspect data as a result of the exercise, and consequently we have not used the associated Voronoi data bins in the modelling process. The bins are not actually removed from the Voronoi tessellations but marked as ‘not in use’.

As identified in Emsellem et al. (2004), the NGC 5846 data contain contamination from a foreground star and a companion (NGC 5846A). This north and south contamination has, as far as possible, been removed by simply deleting all the Voronoi bins where the magnitude of the y -coordinate position is greater than 3.5 kpc.

3.4 Gravitational Potentials

All the galaxies are modelled as axisymmetric galaxies with their gravitational potentials calculated from deprojecting the multi-Gaussian expansions (MGEs) of their surface brightness recorded in Cappellari et al. (2006), and Krajnović et al. (2005) for NGC 2974. The multi-Gaussian expansion technique is described in Emsellem et al. (1994) and is not repeated here. The galactic kinematic and photometric symmetry axes are assumed to align. No M2M modelling of the galaxies with the axes not aligned, as discussed in Emsellem et al. (2007) for example, is undertaken.

In our M2M implementation, to avoid multiple numerical integrations, the MGE potential and associated accelerations are pre-calculated and held on $1500 \times 1500 R - z$ interpolation grids with bilinear interpolation used between grid points. We employ OpenMP² to accelerate production of the grids.

We augment the MGE potential with a central black hole modelled as a Keplerian potential. The mass of the black hole M_{BH} is calculated using the $M_{BH} - \sigma$ relationship as described in Gültekin et al. (2009) (σ is the bulge velocity dispersion). For consistency with Cappellari et al. (2006) we do not include a dark matter component in the potential.

Orbit integration is performed using the standard 2^{nd} order interleaved leap frog method with an adaptive time step. The duration of our M2M models is inversely proportional to the dynamical time of the galaxy being modelled and is numerically, approximately 400 divided by the dynamical time with a minimum of 200 units. We use the formula for dynamical time in Binney & Tremaine (2008) §2.2.2 and calculate it at the half light radius of the model. The size of a galaxy model is 3 times the maximum dispersion in the galaxy’s surface brightness multi-Gaussian expansion. In practice, the model sizes range from 5 to 18 effective radii depending on the galaxy.

3.5 Particle initial conditions

In setting the initial spatial and velocity coordinates for particles, two issues need to be addressed. The first is how to handle global rotation of the galaxy, and the second, how to handle core features. In both cases, we may choose to

take no explicit action and allow the M2M method to attempt to weight the particles such that the observables are reproduced. Alternatively, we may use our knowledge of the galaxy’s features and set the initial particle conditions accordingly. The first approach, taking no explicit action, is inefficient in the use of particles (consider the case of many particles orbiting in the opposite sense to any global rotation - the method will lower the particles’ weights to reduce the particles’ influence on the model observables). We therefore discount the first approach and adopt the second.

We employ two schemes for setting the initial conditions. In the first, we set the initial spatial positions of the particles to approximate the luminosity distribution generated by deprojecting the galaxy’s surface brightness MGE. Creation of the velocity coordinates follows a 3 stage process,

(i) use the velocity dispersions created by solving the semi-isotropic Jeans equations for an axisymmetric system (Binney & Tremaine 2008) to provide initial values for the velocity coordinates,

(ii) set the global rotation sense for a prespecified fraction of the particles to align with the rotation sense of the SAURON observations, and

(iii) for the particles inside the SAURON measurements convex hull, adjust the coordinates to approximate the measured line-of-sight velocity by sampling from a Gaussian distribution formed from the measured line-of-sight velocity and dispersion.

The effect of stage (iii) is to reproduce (approximately) in the particle initial conditions any core features in the SAURON velocity measurements. Determination of the ‘prespecified fraction’ in stage (ii) is not yet an automated process. The fraction is determined iteratively by comparing visually the SAURON velocity contours with the particle equivalents and then adjusting the fraction as necessary. As an example, we show the resulting velocity contours for NGC 2974 in Figure 2.

For the second scheme, a grid-less energy, angular momentum and pseudo third integral system similar to that in Cappellari et al. (2006) is adopted to determine the initial conditions for the particle orbits. We then modify the initial conditions as in stages (ii) and (iii) above. Unless otherwise stated, by default, all modelling runs are performed using this scheme.

We determine the number of particles to be used in our M2M models by examining the particle distribution across the Voronoi bins. We adjust the number of particles such that the minimum mean number of particles per bin is greater than 60. We find that between 10^5 and 5×10^5 particles are required depending on the galaxy. Ideally the minimum number of particles per bin should be used but this would require much larger numbers of particles ($> 10^6$) and correspondingly more computing resources. Note that at any one time during a modelling run significant numbers of particles ($> 30\%$) are outside of the convex hull and are not contributing to reproducing the kinematic observables.

3.6 Kernels

The kernels are similar to those in Long & Mao (2010) and we list them below.

² <http://openmp.org>

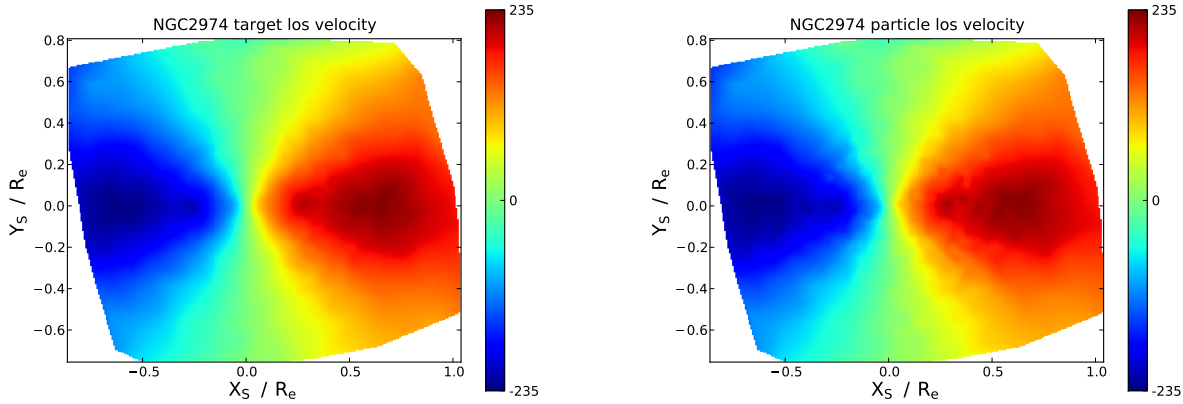


Figure 2. For NGC 2974, the left panel shows the symmetrised measured mean line-of-sight velocity and the right panel, the line-of-sight velocity from the particle initial conditions (at the start of modelling). The velocity units are km s^{-1} .

(i) luminosity density

$$K_{ji} = \frac{L}{V_j} \quad (18)$$

(ii) surface brightness

$$K_{ji} = \frac{L}{A_j} \quad (19)$$

(iii) mean luminosity-weighted Gauss-Hermite coefficient h_n

$$K_{ji} = \frac{\sqrt{2}L}{I_j A_j} H_n(v_{\text{norm},ji}) \exp(-v_{\text{norm},ji}^2/2) \quad (20)$$

where L is the luminosity of the galaxy being modelled, A_j is the area of the bin at position j and I_j the target surface brightness, V_j is the bin volume, $v_{\parallel,i}$ is the line-of-sight velocity for particle i , and H_n is the Hermite polynomial of degree n . The normalised velocity $v_{\text{norm},ji}$ is defined as

$$v_{\text{norm},ji} = \frac{v_{\parallel,i} - \bar{v}_j}{\sigma_j} \quad (21)$$

where \bar{v}_j and σ_j are the measured line-of-sight mean velocity and velocity dispersion respectively. We normalise the Hermite polynomials as described in van der Marel & Franx (1993) appendix A.

3.7 Parameter setting

In this section we describe how we set the values of the various parameters within the M2M method. As indicated earlier, we do not use regularisation for any of the modelling runs and so we take $\mu = 0$. For exponential smoothing we take a common approach across all the galaxies and set $\alpha = 0.05$. The ϵ parameter controls the overall rate of weight evolution and we set $\epsilon = 10^{-4}$ initially. We may alter it later if we find that we are not achieving a χ_k^2 per degree of freedom value of $O(1)$ for a modelling run. Finally, we set $\lambda_{\text{sum}} = 10^4$.

The role of the observable λ_k parameters (see equations 3 and 9) is to help balance the weight evolution equation across all the observables. The equation contains terms of the form

$$\lambda_k \frac{K_{k,ji}}{\sigma_{k,j}} \Delta_{k,j}. \quad (22)$$

The $\Delta_{k,j}$ component reflects how well the model is reproducing the measured observations and is not examined further. The $K_{k,ji}/\sigma_{k,j}$ component varies, by several orders of magnitude, between observables and between positions j for a single observable. By running a M2M model for a short period of time (5 dynamical time units), we are able to understand how the $K_{k,ji}/\sigma_{k,j}$ values are varying. We take the modal value of $K_{k,ji}/\sigma_{k,j}$ (found by binning logarithmically) and set λ_k such that

$$\lambda_k \frac{K_{k,ji}}{\sigma_{k,j}}|_{\text{modal}} = 10. \quad (23)$$

Similarly to ϵ , we may adjust the value of λ_k if we find that we are not achieving a χ_k^2 per degree of freedom value of $O(1)$ for a modelling run.

For the 24 galaxies we analysed, involving some 168 λ_k 's, approximately 25% of the λ_k 's required adjustment. Cappellari et al. (2006) noted that reproducing the Gauss-Hermite coefficient h_4 proved problematic. Based on the $\chi_{h_4}^2$ values we achieve, we do not have an equivalent issue with h_4 .

3.8 Computer performance

Our M2M software has been parallelised using the Message Passing Interface (MPI) with the parallelisation being based around a star network with a single central controlling node. We reported in Long & Mao (2010) that the implementation was highly scaleable and others, for example Dehnen (2009) and de Lorenzi et al. (2007), have reported similarly. This position remains true for a low number of observables and measurement points. However given the number of measurements available for the galaxies we have analysed (see section 3.1), we find that the scaleability is reduced. This reduction in our case is due to the overheads of handling data packet fragmentation particularly on the central node of the network. Increasing the packet size will recover some of the reduction. For larger M2M models, it may be appropriate to introduce a layer of nodes whose primary role is to

act as data concentrators. We have yet to investigate either of these schemes.

3.9 Miscellany

As indicated earlier, this paper builds on Long & Mao (2010) (Paper 1). In this section, we identify various mechanisms and results from that paper, relevant to the current investigation, which have not been dealt with elsewhere.

We use the same weight convergence assessment mechanism as in Paper 1. It is important to note that if a M2M model reproduces the constraining observables, this does not necessarily mean that the particle weights have converged.

We demonstrated in Paper 1 that using regularisation ($\mu \neq 0$) and luminosity density as a constraint made little difference to the model determined mass-to-light ratio. We have chosen not to use regularisation in this paper. Cappellari et al. (2006) did in fact use integral space second derivative regularisation in their mass-to-light exercise. Similarly to regularisation, we choose not to use luminosity density as a constraint on the luminous matter distribution within our M2M models as a matter of course, but include it, where explicitly stated, for comparison purposes only.

For consistency with Cappellari et al. (2006), we quote no confidence intervals on our model determined mass-to-light ratios.

4 MASS-TO-LIGHT DETERMINATION

The process for determining the mass-to-light ratio for a galaxy is straightforward and widely used elsewhere. We run a series of M2M models varying a mass-to-light parameter (Υ) and look for a minimum in the resulting model χ^2 values. The parameter value at the minimum, adjusted for the black hole mass, is taken as the ‘true’ mass-to-light ratio for the galaxy given all the modelling assumptions.

$$\Upsilon_{\text{adjusted}} = \frac{\Upsilon_{\text{model}}L + M_{\text{BH}}}{L} \quad (24)$$

where L is the model total luminosity and M_{BH} is the black hole mass.

The mass-to-light ratios we achieve are shown in Table 1, and Figure 3 contains a plot of the M2M mass-to-light values against those achieved by Cappellari et al. (2006) using Schwarzschild’s method. For 96% of the galaxies, the relative difference between the mass-to-light values is $< 20\%$ and for 83% of the galaxies, the difference is $< 10\%$. 3 galaxies have differences $> 15\%$ - NGC 524 (28%), NGC 4486 (16%), and NGC5845 (17%). Table 2 contains a fuller breakdown.

Performing a least squares straight line fit to the logarithmic mass-to-light data yields

$$\Upsilon_{\text{M2M}} \propto \Upsilon_{\text{Sch}}^{1.11 \pm 0.04} \quad (25)$$

where Υ_{M2M} is the M2M mass-to-light ratio and Υ_{Sch} is the Schwarzschild equivalent. Introducing luminosity density to constrain the distribution of luminous matter does not alter this relationship. (For most galaxies, the models already well reproduce the density without the use of an explicit constraint). Changing the particle initial conditions to scheme 1 in section 3.5 (match the luminosity density spatially, velocities based on the Jeans’ equations) does not significantly alter the relationship with

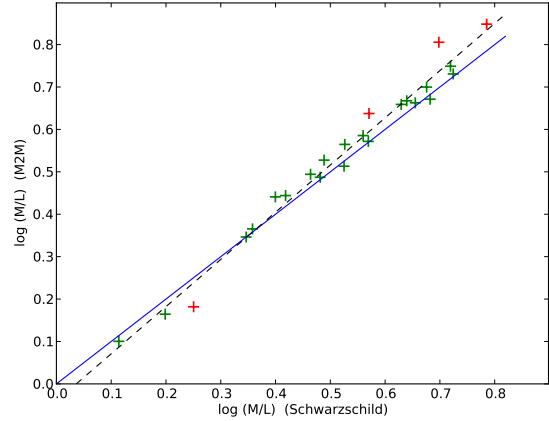


Figure 3. Comparison of M2M vs Schwarzschild mass-to-light ratios with galaxies which differ by more than 10% marked in red. The solid blue line represents equality of the ratios, and the black dashed line a least squares fit to the data.

Table 2. Comparison between M2M and SAURON mass-to-light ratios

Difference	Number of galaxies	Galaxy NGC numbers
$< 5\%$	9	38% 2974, 3377, 3608, 4150, 4458, 4526, 4621, 5813, 5846
5% to 10%	11	46% 821, 3156, 3379, 3414, 4278, 4374, 4459, 4473, 4550, 4552, 4660
10% to 15%	1	4% 7457
$> 15\%$	3	13% 524, 4486, 5845

$$\Upsilon_{\text{M2M}} \propto \Upsilon_{\text{Sch}}^{1.18 \pm 0.05}. \quad (26)$$

Removing NGC 524 as an ‘outlier’ in the M2M results, we calculate the root mean square deviation of the two sets of mass-to-light ratios as 0.31. Assuming the errors in both the Schwarzschild and M2M methods to be similar, we arrive at an intrinsic error in the methods of 5.9% (calculated as the rms deviation divided by $\sqrt{2}$ divided by the mean M2M mass-to-light ratio). This figure agrees well with the value (6%) quoted by Cappellari et al. (2006) for their comparison of Jeans and Schwarzschild models, and with the theoretical model values ($\approx 5\%$) achieved in Long & Mao (2010).

Despite differences in the two modelling methods, in general the methods are delivering, as one would hope, similar mass-to-light ratios for a galaxy. However, it is apparent from Figure 3 that, for the sample of galaxies analysed, either the M2M method is slightly over-estimating the mass-to-light ratios, or conversely, that Schwarzschild’s method is under-estimating them.

Having determined an estimate for the galaxies’ mass-to-light ratios, we perform a further set of modelling runs at those ratios using 10^6 particles in order to investigate how well the observables are reproduced and to calculate the global anisotropy parameters (see section 5). At the estimated mass-to-light ratios, weight convergence is good with

Table 3. χ^2 per degree of freedom analysis - all galaxies

Observable	Minimum χ^2/dof	Maximum χ^2/dof	Mean χ^2/dof	Median χ^2/dof
sb	0.05	0.64	0.30	0.25
h_1	0.05	0.96	0.35	0.27
h_2	0.39	1.22	0.73	0.75
h_3	0.19	2.17	0.58	0.50
h_4	0.36	1.20	0.66	0.61
h_5	0.000	0.023	0.004	0.001
h_6	0.002	0.021	0.009	0.008
v_m	0.05	0.97	0.35	0.27
σ_m	0.33	2.31	0.78	0.70

The M2M constraining observables are surface brightness (sb) and h_1 to h_6 . The model mean line-of-sight velocity (v_m) and velocity dispersion (σ_m) are calculated as in equations 16 and 17. The maximum values of h_3 and v_m come from the modelling of NGC 5845 and the maximum of σ_m from NGC 3156.

$\approx 98\%$ of particles having converged weights. The χ^2 per degree of freedom values for the constraining observables (surface brightness and the Gauss-Hermite coefficients h_1 to h_6) are generally less than 1. The values for the calculated observables (mean line-of-sight velocity and velocity dispersion) are similarly so. More detail is given in Table 3. In Figure 4, we show the observed and model line-of-sight velocity maps for a selection of 4 galaxies (NGC 2974, NGC 3414, NGC 4550 and NGC 5813) covering the major galaxy types (elliptical and lenticular), rotation (fast and slow), orientation (inclined to the line-of-sight and edge-on) and core features. In particular, we note that the M2M method is able to reproduce kinematically distinct cores and counter rotating cores. For completeness, Figure 5 contains a complete set of observable maps (velocity, dispersion, h_3 , and h_4) for NGC 4660. Overall, reproduction is satisfactory.

5 ANISOTROPY PARAMETERS

5.1 Theory

The global anisotropy parameter δ is given in Binney & Tremaine (2008) §4.8 and Cappellari et al. (2007) as

$$\delta = 1 - \frac{\Pi_{zz}}{\Pi_{xx}} \quad (27)$$

where Π_{ij} is from the kinetic energy due to random stellar motion, z indicates the symmetry axis of an axisymmetric galaxy and x is some fixed direction orthogonal to it. Π_{kk} is defined as

$$\Pi_{kk} = \int \rho \sigma_k^2 d^3 \mathbf{x} \quad (28)$$

where ρ is the mass density and σ_k the velocity dispersion in direction k . The equivalent for M2M modelling purposes, calculated using the particle weights and binning particle data into J bins, is

$$\Pi_{kk} = \Upsilon L \sum_j^J W_j \sigma_{k,j}^2 \quad (29)$$

where Υ is the mass-to-light ratio of the galaxy, L is the model luminosity, $\sigma_{k,j}$ is the mean luminosity weighted velocity dispersion in direction k in bin j , and W_j , the sum of the particles weights in bin j , is given by

$$W_j = \sum_i^N w_i \delta(i \in j). \quad (30)$$

Cappellari et al. (2007) introduce two further parameters, β and γ . Using cylindrical polar coordinates (R, ϕ, z),

$$\beta = 1 - \frac{\Pi_{zz}}{\Pi_{RR}} \quad (31)$$

and

$$\gamma = 1 - \frac{\Pi_{\phi\phi}}{\Pi_{RR}}. \quad (32)$$

The global anisotropy parameter δ is then calculated as

$$\delta = \frac{2\beta - \gamma}{2 - \gamma}. \quad (33)$$

As noted in Cappellari et al. (2007), β describes the global shape of the velocity dispersion tensor in the (v_R, v_z) plane, and γ the shape in a plane orthogonal to v_z .

The three anisotropy parameters described so far, whilst still applicable to spherical galaxies, are more appropriate to axisymmetric galaxies. Cappellari et al. (2007) describe a further parameter, β_r , to measure the anisotropy of (near) spherical galaxies.

$$\beta_r = 1 - \frac{\Pi_{\theta\theta} + \Pi_{\phi\phi}}{2 \Pi_{rr}} \quad (34)$$

where (r, θ, ϕ) are spherical coordinates.

For all parameters, the radial and tangential velocity dispersion anisotropy regimes are shown in Figure 6. For the directions indicated within the definitions of the parameters, a zero parameter value indicates isotropy and a positive value, a radial bias to the velocity dispersion.

5.2 M2M modelling

For each galaxy, we perform a M2M modelling run using the mass-to-light ratio determined in section 4. We calculate the anisotropy parameters by binning the end of run particle velocity data on an (R, z) grid for β and γ , and for β_r , we bin the data radially. Given we are using the particle data directly, the number of particles is increased to 1×10^6 . Similarly to Cappellari et al. (2007), we only include particles in the calculation which are currently within 25 arcsec spherical radius of the galactic centre.

Overall, we achieve reasonable (but not good) agreement with the SAURON values of the global anisotropy parameter δ with 14 of the 24 galaxies having M2M values equal to $\delta_{\text{SAURON}} \pm 0.05$. The detailed results are captured in Table 4. Figure 6 shows β , γ and β_r plotted against δ and is the equivalent of Cappellari et al. (2007) Figure 2. Figures 7 and 8 compare the M2M parameter values against the SAURON values. Two main differences can be seen, the first being that in the M2M results the slow rotating galaxies are more clustered in parameter space. The second is that from Figure 6 the number of galaxies exhibiting tangential anisotropy has reduced and we examine this in more detail below.

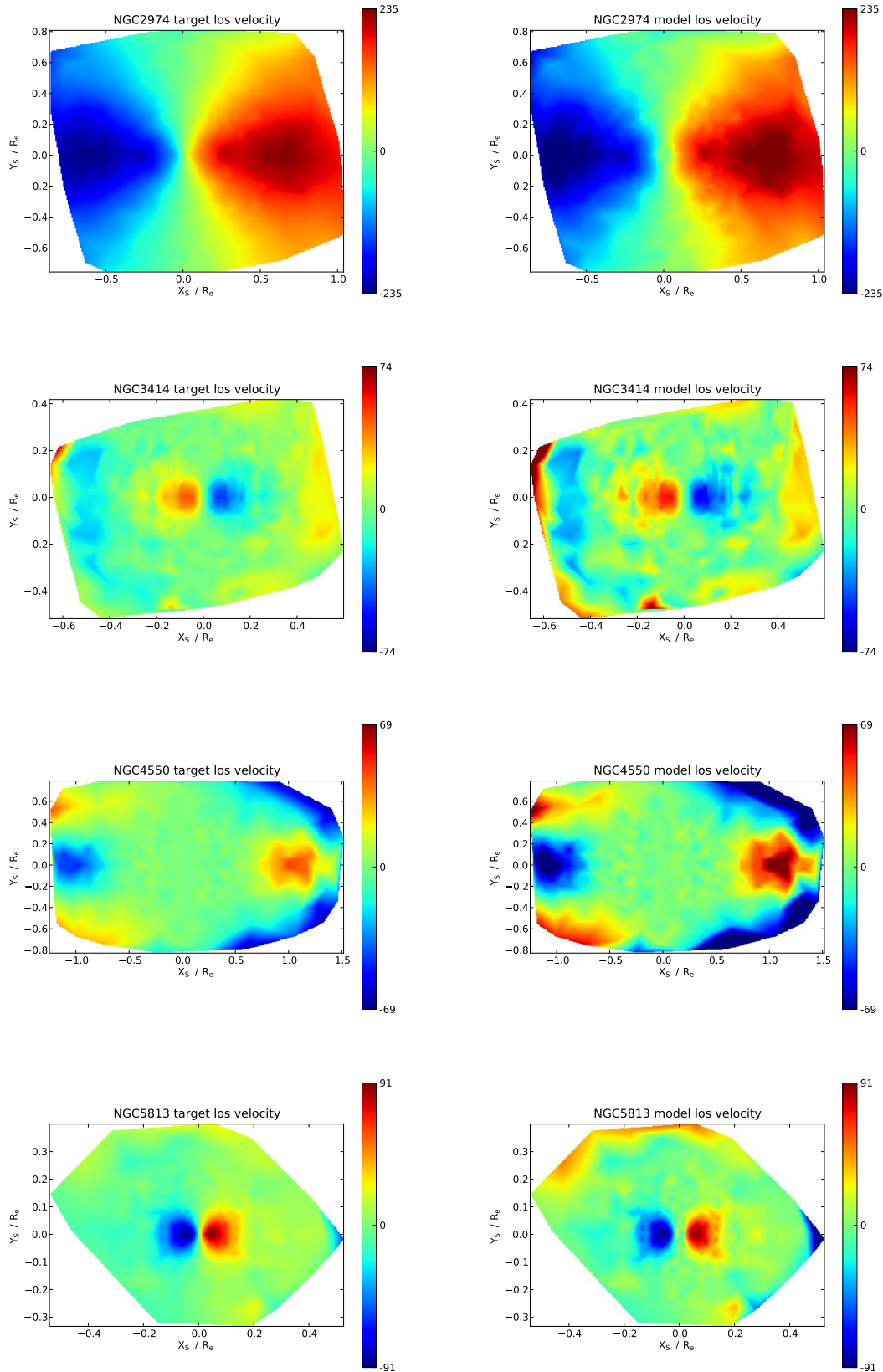


Figure 4. Galaxy velocity maps for NGC 2974 (inclined, elliptical, fast rotator), NGC 3414 (edge-on, lenticular, slow rotator with a counter rotating core), NGC 4550 (inclined, lenticular, fast rotator with counter rotating disc) and NGC 5813 (edge-on, elliptical, slow rotator with a kinematically distinct core) showing the target mean line-of-sight velocity and the model produced versions. See Table 1 for more data on the individual galaxies. The velocity units are km s^{-1} .

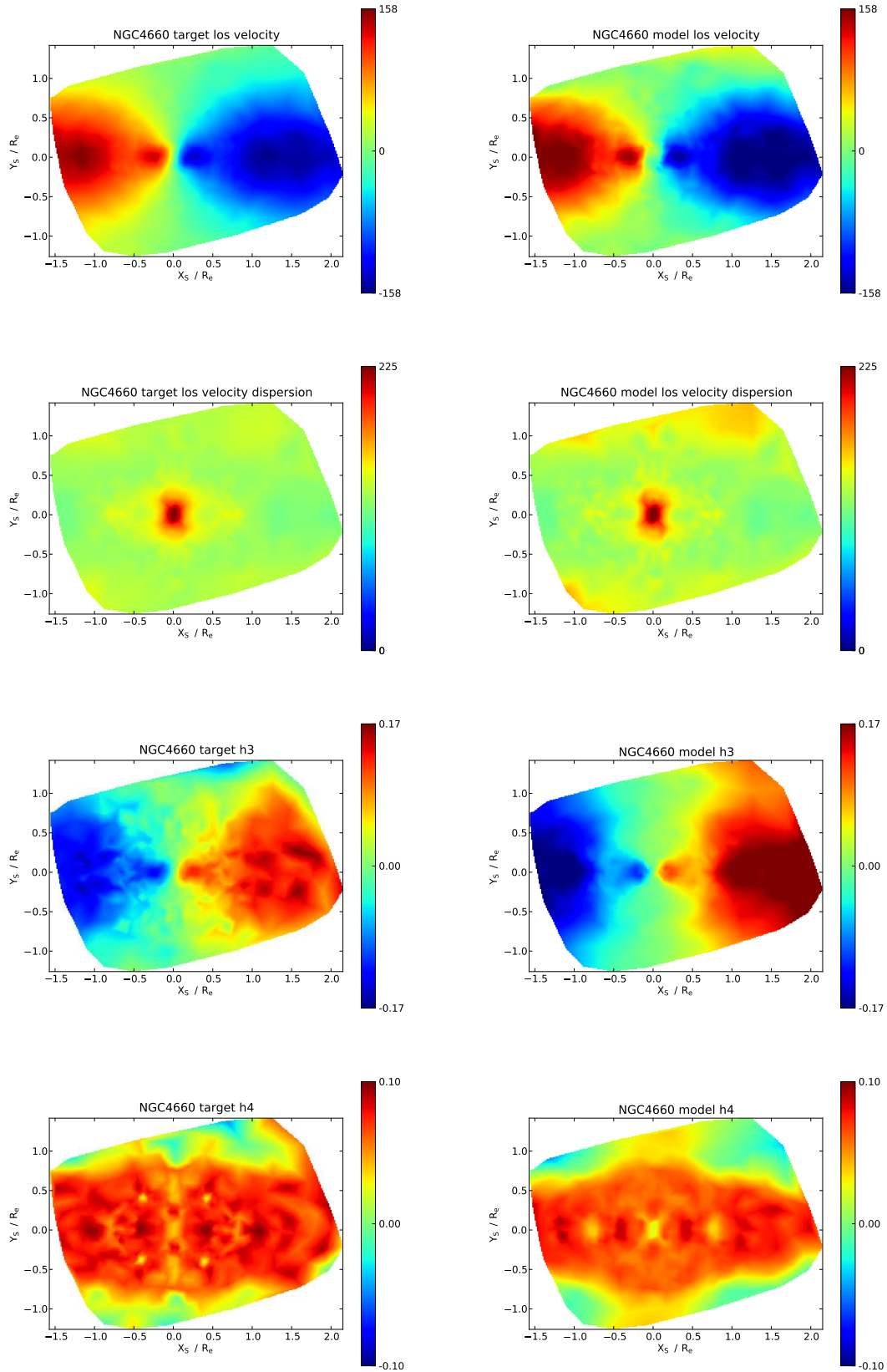


Figure 5. The complete set of target and model observable maps for NGC 4660.

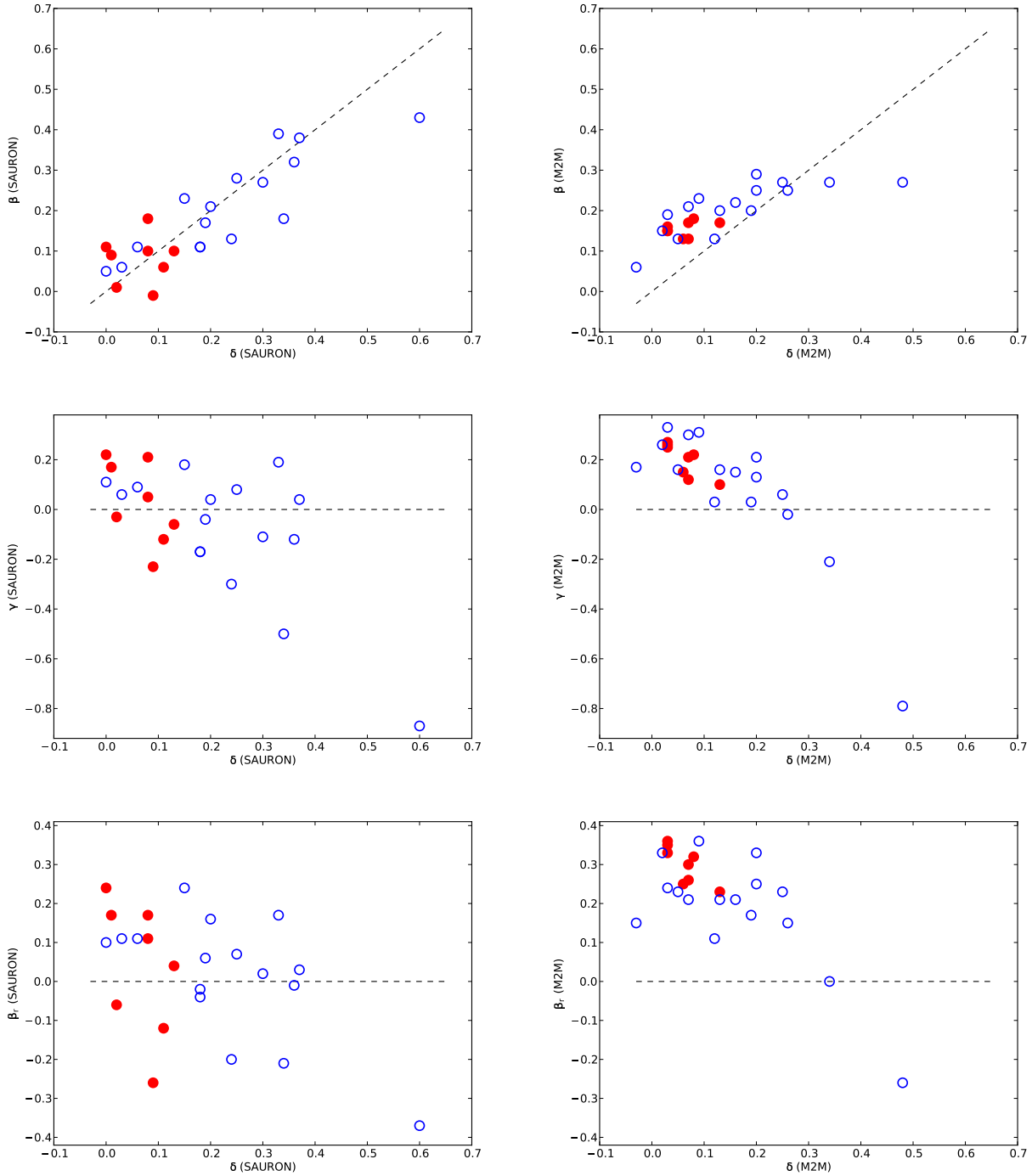


Figure 6. Anisotropy parameters β , γ and β_r for the individual galaxies plotted against δ . Slow rotating galaxies are plotted with red solid markers. The M2M plots are in the right hand column. Plots from Cappellari et al. (2007) (left hand column) have been included for comparison purposes. The black dashed lines separate the plot areas into radial (upper or upper left) and tangential (lower or lower right) anisotropy regimes. It is clear that fewer M2M models exhibit tangential velocity dispersion anisotropy and that the slow rotating galaxies are more tightly clustered in parameter space than their SAURON equivalents.

We start by performing a simple count of the number of positive and negative parameter values - the result is recorded in Table 5. For the fast rotating galaxies, any change of sign of a parameter between the SAURON and M2M values comes from one of 6 galaxies (NGC 2974, 4150,

4278, 4473, 4621, 4660). Similarly, for slow rotating galaxies, only 4 galaxies are involved (NGC 3414, 3608, 4458, 4552). From examining the characteristics of the galaxies, there are no obvious groupings which might help explain the differences between the SAURON and M2M results. For

Table 4. Comparison between SAURON and M2M anisotropy parameters

Galaxy	Inclination (deg)	Fast Rotator	Cappellari et al. (2007)				From M2M models			
			β_r	β	γ	δ	β_r	β	γ	δ
NGC 524	19	yes	0.06	0.17	-0.04	0.19	0.00	0.27	-0.21	0.34
NGC 821	90	yes	0.16	0.21	0.04	0.20	0.25	0.25	0.13	0.20
NGC 2974	57	yes	-0.20	0.13	-0.30	0.24	0.11	0.13	0.03	0.12
NGC 3156	68	yes	0.17	0.39	0.19	0.33	0.24	0.19	0.33	0.03
NGC 3377	90	yes	0.07	0.28	0.08	0.25	0.21	0.22	0.15	0.16
NGC 3379	90	yes	0.11	0.06	0.06	0.03	0.33	0.15	0.26	0.02
NGC 3414	90	no	-0.12	0.06	-0.12	0.11	0.25	0.13	0.15	0.06
NGC 3608	90	no	0.04	0.10	-0.06	0.13	0.23	0.17	0.10	0.13
NGC 4150	52	yes	-0.01	0.32	-0.12	0.36	0.15	0.06	0.17	-0.03
NGC 4278	90	yes	-0.02	0.11	-0.17	0.18	0.33	0.29	0.21	0.20
NGC 4374	90	no	0.11	0.10	0.05	0.08	0.30	0.17	0.21	0.07
NGC 4458	90	no	-0.26	-0.01	-0.23	0.09	0.26	0.13	0.12	0.07
NGC 4459	47	yes	0.10	0.05	0.11	0.00	0.23	0.13	0.16	0.05
NGC 4473	73	yes	-0.21	0.18	-0.50	0.34	0.15	0.25	-0.02	0.26
NGC 4486	90	no	0.24	0.11	0.22	0.00	0.35	0.15	0.26	0.03
NGC 4526	79	yes	0.11	0.11	0.09	0.06	0.21	0.20	0.16	0.13
NGC 4550	84	yes	-0.37	0.43	-0.87	0.60	-0.26	0.27	-0.79	0.48
NGC 4552	90	no	-0.06	0.01	-0.03	0.02	0.33	0.16	0.27	0.03
NGC 4621	90	yes	-0.04	0.11	-0.17	0.18	0.17	0.20	0.03	0.19
NGC 4660	70	yes	0.02	0.27	-0.11	0.30	0.23	0.27	0.06	0.25
NGC 5813	90	no	0.17	0.18	0.21	0.08	0.32	0.18	0.22	0.08
NGC 5845	90	yes	0.24	0.23	0.18	0.15	0.36	0.23	0.31	0.09
NGC 5846	90	no	0.17	0.09	0.17	0.01	0.36	0.15	0.25	0.03
NGC 7457	64	yes	0.03	0.38	0.04	0.37	0.21	0.21	0.30	0.07

Comparison between the SAURON values for the anisotropy parameters β_r , β , γ and δ taken from Cappellari et al. (2007) Table 2, and the same parameters calculated from M2M models. For the δ parameter, 14 M2M values (including all the slow rotating galaxies) are within ± 0.05 of the SAURON values.

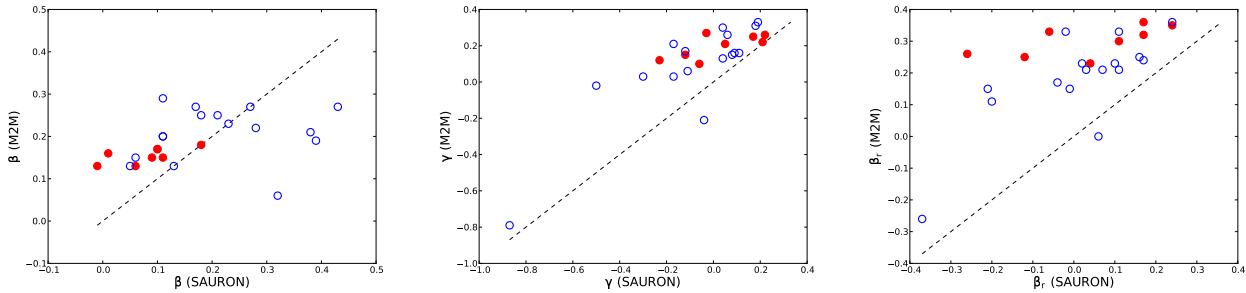


Figure 8. Comparison between the M2M and SAURON determined anisotropy parameters β , γ and β_r . Slow rotating galaxies are plotted with red solid markers. The black dashed lines indicate equality of the M2M and SAURON values.

example, the 10 galaxies include both elliptical and lenticular galaxies and galaxies which are inclined to the line-of-sight or edge-on. All the galaxies have M2M mass-to-light ratios which differ from the SAURON values by $< 7.5\%$, and 7 of the galaxies have M2M δ anisotropy parameter values within ± 0.05 of the SAURON values. It should be noted that for a given value of the global anisotropy parameter δ , there is a linear relationship between β and γ so a range of orbital models and velocity dispersion anisotropies is to be expected given the kinematic observations available. Including luminosity density as a constraint does not alter the tangential anisotropy result. Note that the data used in Cappellari et al. (2007) (see section 2) differ from

the SAURON data release though it is not clear that this would explain the differences.

In the absence of further constraints and perhaps more detailed investigations, we conclude that the differences in the anisotropy parameter values are due to differences in the particle / orbit initial conditions and the modelling methods used resulting in different orbital weightings.

6 CONCLUSIONS

We have undertaken the largest M2M exercise to date and re-analysed 24 elliptical and lenticular galaxies previously analysed with Schwarzschild's method. We have used the

Table 5. Anisotropy parameter analysis

Parameter	Number of Positive Values		Number of Negative Values		Galaxy NGC numbers
	Sauron	M2M	Sauron	M2M	
Fast Rotators					
β_r	10	15	6	1	2974, 4150, 4278, 4473, 4621
β	16	16	0	0	
γ	8	13	8	3	2974, 4150, 4278, 4621, 4660
δ	16	15	0	1	4150
Slow Rotators					
β_r	5	8	3	0	3414, 4458, 4552
β	7	8	1	0	4458
γ	4	8	4	0	3414, 3608, 4458, 4552
δ	8	8	0	0	

The table shows the numbers of galaxies with positive and negative velocity dispersion anisotropy parameter values as a means of assessing any general change of radial or tangential anisotropy regime for the sample of galaxies. The ‘galaxy’ column indicates those galaxies where the regime differs between the SAURON and M2M models.

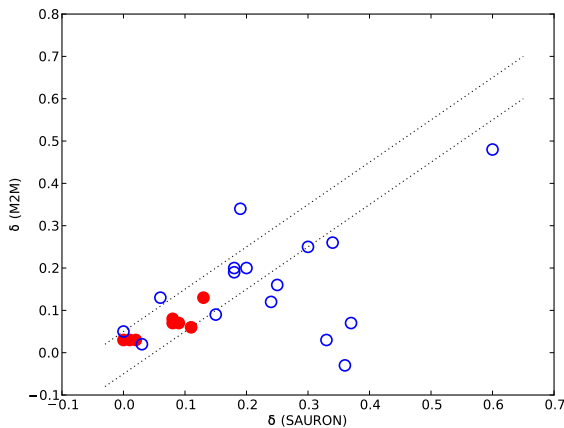


Figure 7. Comparison between the M2M and SAURON determined values of the global anisotropy parameter δ . Slow rotating galaxies are plotted with red solid markers. The black dotted lines indicate ± 0.05 of the SAURON values recorded in Cappellari et al. (2007).

M2M method as far as possible as a ‘black box’ - we have developed no computer code specific to any one galaxy. Where there are modelling parameters to be set or tuned, we have adopted the same strategy and process for all galaxies.

Our M2M implementation has been adapted to use observable data available as a Voronoi tessellation and to handle gravitational potentials derived from a multi-Gaussian expansion and deprojection of a galaxy’s surface brightness. We have identified a computer performance issue with our M2M implementation which may affect other users of the method depending on their implementation and network configuration. For the future, an improved process, preferably computerised, for setting the global rotation of the system of particles is required.

We achieve reasonable agreement (14 out of 24 galaxies) with the SAURON values of the global anisotropy parameter δ but our overall assessment is that further (theoretical) investigations of the impact of orbit / particle initial conditions and the resultant orbit weights are required before the

differences between the SAURON and M2M methods can be fully understood. In the M2M case, it may prove to better to calculate an exponentially smoothed version of δ rather than relying on the end of modelling run particle data.

We have demonstrated that, despite differences in the M2M and Schwarzschild modelling methods, in general the methods are delivering similar mass-to-light ratios for a galaxy. Whether the slight over estimation (M2M) or under estimation (Schwarzschild) is a real effect or not will only be resolved by using a different sample of galaxies.

ACKNOWLEDGEMENTS

The authors gratefully acknowledge the advice, help and support provided by Michele Cappellari, and thank John Magorrian for an enlightening discussion on Gauss-Hermite series. The final computer runs were performed on the *Laohu* high performance computer cluster of the National Astronomical Observatories, Chinese Academy of Sciences, with earlier runs being performed on the Jodrell Bank Centre for Astrophysics, University of Manchester, *Coma* cluster.

REFERENCES

- Binney J., Tremaine S., 2008, *Galactic Dynamics: Second Edition*. Princeton University Press
- Cappellari M., Bacon R., Bureau M., Damen M. C., Davies R. L., de Zeeuw P. T., Emsellem E., Falcón-Barroso J., Krajnović D., Kuntschner H., McDermid R. M., Peletier R. F., Sarzi M., van den Bosch R. C. E., van de Ven G., 2006, *MNRAS*, 366, 1126
- Cappellari M., Copin Y., 2003, *MNRAS*, 342, 345
- Cappellari M., Emsellem E., Bacon R., Bureau M., Davies R. L., de Zeeuw P. T., Falcón-Barroso J., Krajnović D., Kuntschner H., McDermid R. M., Peletier R. F., Sarzi M., van den Bosch R. C. E., van de Ven G., 2007, *MNRAS*, 379, 418
- Das P., Gerhard O., Mendez R. H., Teodorescu A. M., de Lorenzi F., 2011, *MNRAS*, 415, 1244

- de Lorenzi F., Debattista V. P., Gerhard O., Sambhus N., 2007, *MNRAS*, 376, 71
- de Lorenzi F., Gerhard O., Coccato L., Arnaboldi M., Cappaccioli M., Douglas N. G., Freeman K. C., Kuijken K., Merrifield M. R., Napolitano N. R., Noordermeer E., Romanowsky A. J., Debattista V. P., 2009, *MNRAS*, 395, 76
- de Lorenzi F., Gerhard O., Saglia R. P., Sambhus N., Debattista V. P., Pannella M., Méndez R. H., 2008, *MNRAS*, 385, 1729
- Dehnen W., 2009, *MNRAS*, 395, 1079
- Emsellem E., Cappellari M., Krajnović D., van de Ven G., Bacon R., Bureau M., Davies R. L., de Zeeuw P. T., Falcón-Barroso J., Kuntschner H., McDermid R., Peletier R. F., Sarzi M., 2007, *MNRAS*, 379, 401
- Emsellem E., Cappellari M., Peletier R. F., McDermid R. M., Bacon R., Bureau M., Copin Y., Davies R. L., Krajnović D., Kuntschner H., Miller B. W., de Zeeuw P. T., 2004, *MNRAS*, 352, 721
- Emsellem E., Monnet G., Bacon R., 1994, *AAP*, 285, 723
- Gültekin K., Richstone D. O., Gebhardt K., Lauer T. R., Tremaine S., Aller M. C., Bender R., Dressler A., Faber S. M., Filippenko A. V., Green R., Ho L. C., Kormendy J., Magorrian J., Pinkney J., Siopis C., 2009, *APJ*, 698, 198
- Jalali M. A., Tremaine S., 2011, *MNRAS*, 410, 2003
- Jourdeuil E., Emsellem E., 2007, in Kissler-Patig M., Walsh J. R., Roth M. M., eds, *Science Perspectives for 3D Spectroscopy Scalable N-body Code for the Modeling of Early-type Galaxies*. pp 99–103
- Krajnović D., Cappellari M., Emsellem E., McDermid R. M., de Zeeuw P. T., 2005, *MNRAS*, 357, 1113
- Long R. J., Mao S., 2010, *MNRAS*, 405, 301
- Magorrian J., Binney J., 1994, *MNRAS*, 271, 949
- Rix H.-W., de Zeeuw P. T., Cretton N., van der Marel R. P., Carollo C. M., 1997, *APJ*, 488, 702
- Rodionov S. A., Athanassoula E., Sotnikova N. Y., 2009, *MNRAS*, 392, 904
- Schwarzschild M., 1979, *APJ*, 232, 236
- Syer D., Tremaine S., 1996, *MNRAS*, 282, 223
- van den Bosch R. C. E., van de Ven G., Verolme E. K., Cappellari M., de Zeeuw P. T., 2008, *MNRAS*, 385, 647
- van der Marel R. P., Franx M., 1993, *APJ*, 407, 525